

An explicit elastic solution for a brittle film with periodic cracks

H. M. Yin · G. H. Paulino · W. G. Buttlar

Received: 5 August 2008 / Accepted: 12 November 2008 / Published online: 16 December 2008
© Springer Science+Business Media B.V. 2008

Abstract A two-dimensional explicit elastic solution is derived for a brittle film bonded to a ductile substrate through either a frictional interface or a fully bonded interface, in which periodically distributed discontinuities are formed within the film due to the applied tensile stress in the substrate and consideration of a “weak form stress boundary condition” at the crack surface. This solution is applied to calculate the energy release rate of three-dimensional channeling cracks. Fracture toughness and nominal tensile strength of the film are obtained through the relation between crack spacing and tensile strain in the substrate. Comparisons of this solution with finite element simulations show that the proposed model provides an accurate solution for the film/substrate system with a frictional interface; whereas for a fully bonded interface it produces a good prediction only when the substrate is not overly compliant or when the crack spacing is large compared with the thickness of the film. If the section is idealized as infinitely long, this solution in terms of the energy release rate recovers Beuth’s exact solution for a fully

cracked film bonded to a semi-infinite substrate. Interfacial shear stress and the edge effect on the energy release rate of an asymmetric crack are analyzed. Fracture toughness and crack spacing are calculated and are in good agreement with available experiments.

Keywords Energy release rate · Elastic materials · Fracture toughness · Thin film · Channeling crack · Periodic cracks

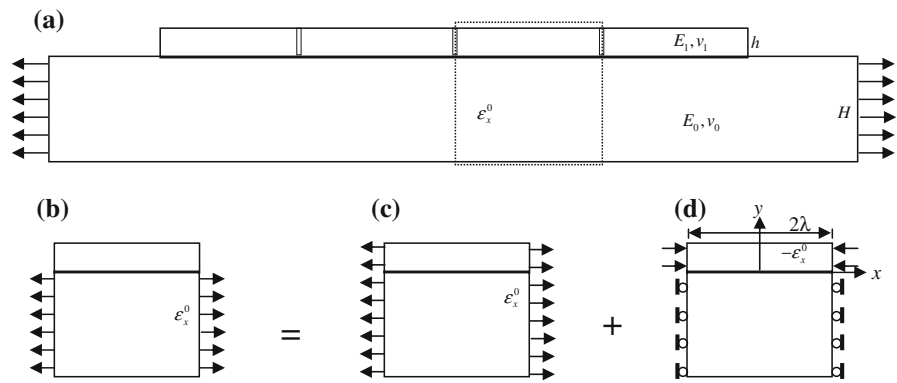
1 Introduction

A brittle film or coating bonded to a substrate that is subjected to a tensile stress may fail by the formation of a series of uniformly distributed cracks in the longitudinal direction of the film (Fig. 1a). With increased tensile stress, additional cracks form until the saturation spacing is achieved (Agrawal and Raj 1989; Hutchinson and Suo 1992). This mechanism has been used to evaluate the interfacial shear strength (Agrawal and Raj 1989) and to measure the elastic modulus and the fracture toughness of the film (Thouless et al. 1992; Wang et al. 1998). A number of experiments have been developed to study the dependence of fracture behavior on the geometry of the film, the mechanical properties of the film and substrate, and conditions of the interface (see, for example, Hu and Evans 1989; Bordet et al. 1998; Etkorn and Clarke 2001; Alaca et al. 2002; Zhao et al. 2002; Malzbender 2004; Tadepalli et al. 2008).

H. M. Yin (✉)
Department of Civil Engineering and Engineering
Mechanics, Columbia University, 610 Seeley W. Mudd,
500 West 120th Street, New York, NY 10027, USA
e-mail: yin@civil.columbia.edu

G. H. Paulino · W. G. Buttlar
Department of Civil and Environmental Engineering,
University of Illinois at Urbana-Champaign, Newmark
Laboratory, 205 North Mathews Avenue, Urbana,
IL 61801, USA

Fig. 1 A brittle film resting on a thick substrate with uniformly distributed discontinuities due to a uniform strain in the substrate: **a** the discontinuity map; **b** the marked section between two discontinuities; **c** the uniformly strained section; **d** the section with the ends of the film compressed and the ends of the constrained substrate



Crack propagation in a thin film exhibits a three-dimensional (3D) process. When the local stress reaches a critical value, a crack initiates perpendicular to the film surface and spreads by channeling across the thickness of the film (Beuth 1992; Xia and Hutchinson 2000; Vlassak 2003). Nakamura and Kamath (1992) presented a 3D finite element analysis (FEA) and showed that the channeling crack reaches a steady-state when the crack length is more than twice the film thickness for a film bonded to a rigid substrate. The elastic fields due to a steady-state channeling crack are typically solved by a two-dimensional (2D) plane strain analysis. Because a singular point exists at the crack tip, which is located at the bottom of the film, many analyses have focused on the local elastic solution in the neighborhood of that point. Beuth (1992) presented solutions of fully and partially cracked film problems for elastic films bonded to elastic substrates. Beuth and Klingbeil (1996) extended this work to elastic-plastic substrates by using the simple shear lag model (Hu and Evans 1989). In addition, Liu et al. (1999) and Yu et al. (2001) investigated the elastic field due to the edge effects. Although local solutions such as these are useful in the study of crack propagation, they cannot be directly used to predict crack initiation, crack spacing, or to study the interaction between cracks. The overall elastic field is essential to provide a complete picture of cracking in films.

To analyze the interfacial shear strength, Agrawal and Raj (1989) employed a sine wave function to approximate the shear stress along the interface. Saif et al. (1993) adopted the simple shear lag model and the 2D finite element method (FEM) to analyze stress distributions in the whole film. Chen et al. (2000) also obtained the stress distribution by 2D FEM and demonstrated that Agrawal and Raj (1989) approxima-

tion is not reasonable in the vicinity of discontinuities. Xia and Hutchinson (2000) and Shenoy et al. (2001), respectively, proposed an elastic solution in integral forms. Parmigiani and Thouless (2006) employed a cohesive zone model to simulate crack deflection at interfaces. Fleck and Qiu (2007) used linear FEM to study the damage tolerance of 2D isotropic lattices. Numerical methods are a good tool to solve the elastic field, however, they do not lead to a general solution for the class of problems of interest.

Timm et al. (2003) developed a one-dimensional (1D) closed-form solution for an elastic strip on a substrate with a frictional interface, in which the shear stress is balanced by a uniform tensile stress along the thickness of the strip. However, because the friction forces are driven from the interface, the tensile stress and the shear stress will significantly change along the thickness. Obviously, a 1D solution cannot describe the stress distribution variation along the thickness. Thus, a 2D model is necessary to better analyze the stress distribution of the film.

The purpose of this paper is to solve the elastic field distribution in a 2D brittle film bonded to a substrate and subjected to uniform tensile strain in the substrate as seen in Fig. 1a. The film is assumed to be fully bonded to the substrate even during the formation of the discontinuities, and thus no delamination along the interface is considered. Because the film is thin and brittle, once a crack initiates, it is assumed to propagate across the thickness of the film and stop at the interface. The cracks in the substrate are not considered. By using the specific boundary and loading conditions, a general solution for the elastic fields of the film is obtained in a closed form for two kinds of interfaces: a frictional interface and a fully bonded interface.

When the width of the film is very large, the cracks spread by channeling normal to the loading direction. The energy release rate of a steady-state channeling crack is obtained as the work done to close the crack far behind the crack tip (Beuth 1992). If the width of the film is limited, the channeling process may be unstable (Hutchinson and Suo 1992), and cracks will quickly spread across the width and thickness, and thus some discontinuities form. The fracture toughness can be solved as the critical energy release rate at the formation of the discontinuity. The nominal tensile strength not only depends on fracture energy and elastic moduli of the film material, but also changes with the crack spacing and the thickness of the film.

The interfacial shear stress is explicitly given for two kinds of interfaces. For a very thin film, the shear stress is only concentrated in the neighborhood of the crack tip, and is quickly reduced to zero far from the singular point. If the interfacial shear strength is given, a method for evaluating the propensity for debonding along the interface in the vicinity of discontinuities is presented. Furthermore, a fully bonded interface can be simulated by a frictional interface by introducing an equivalent spring coefficient. A thinner film provides a higher equivalent spring coefficient. This 2D solution is compared with Xia and Hutchinson's (2000) results obtained from 1D solution, which shows that the proposed solution leads to a clearer physical meaning.

The edge effect on the energy release rate is further discussed. When a long film/substrate system is subjected to a tensile stress in the substrate, in the beginning, many cracks may simultaneously initiate in the middle range. When the length of the section between discontinuities is small enough, a new crack will initiate at the symmetric plane so that the section is cracked into two equal pieces. Thus, the film will finally be cracked into pieces with roughly equal length. When a film/substrate system is subjected to a fixed tensile strain in the substrate, fracture toughness is calculated and compared with the experimental data. The proposed solution provides a reasonable explanation of the experimental observation: given fracture toughness and tensile loading in a film/substrate system, there exists a critical thickness, below which no crack initiates.

The remainder of this paper is organized as follows. Section 2 presents the general solution of the displacement field in a periodic section between two discontinuities and provides the explicit expressions of the elastic fields for the film/substrate system with two kinds of

interfaces. Section 3 emphasizes the energy release rate of a channeling crack and provides a method to measure the fracture toughness and nominal tensile strength of the film. Section 4 shows some comparisons with FEM simulations and validates the accuracy of the proposed solution. Applying this solution, we also investigate the interfacial shear stress distribution, equivalent spring coefficient of the fully bonded interface, and edge effect on the energy release rate of an asymmetric crack. The proposed method is shown to be in good agreement with the experimental results of Thouless et al. (1992).

2 Basic formulation

Consider a brittle film (thickness h , Young's modulus E_1 , Poisson's ratio ν_1) bonded to a thick substrate (thickness H , Young's modulus E_0 , Poisson's ratio ν_0) as illustrated in Fig. 1a. With the increase of the tensile strain in the substrate (the averaged strain denoted by ε_x^0), some uniformly distributed discontinuities form across the thickness of the film. However, the tensile strain on the ends of each section is still assumed to be uniform along the depth of the substrate and equal to the averaged strain of the substrate as ε_x^0 . Based on the periodic boundary condition, the section highlighted in Fig. 1a is selected to represent all other sections. When the tensile strain reaches ε_x^0 , the marked section of the film with length 2λ will be cracked into two pieces. To solve the elastic field in the section at the moment just before the crack forms (Fig. 1b), a standard representation introduced for analysis purposes employs the superposition of a uniformly strained section (Fig. 1c) with the "reduced problem" (Fig. 1d) wherein the film is bonded to the substrate and subjected to a uniform compressive strain $-\varepsilon_x^0$ on its ends (Yu et al. 2001). To make the total averaged strain of the substrate consistent, the x -directional displacements at the ends of the substrate in Fig. 1d are constrained. Because the deformation of Fig. 1c is compatible between the film and the substrate, the strain field in the film is still uniform as ε_x^0 . To solve the reduced problem, a 2D Cartesian coordinate system is setup with the origin at the central bottom of the section. A plane strain problem is considered.

Because the thickness of the film is much smaller than its length and the top surface is free, generally the top surface of the film remains approximately flat

during the compression if no debonding happens along the interface between the film and the substrate. Thus, it is assumed that all points of a plane normal to the y direction is still in the same plane after deformation (Yin et al. 2007), i.e.,

$$u_y(x, y) = u_y(y). \quad (1)$$

The constitutive law in the plane strain problem reads

$$\sigma_x = \bar{E}_1 u_{x,x}, \quad \tau_{xy} = \mu_1 u_{x,y}, \quad (2)$$

where the elastic moduli are denoted as $\bar{E}_1 = E_1/(1 - \nu_1^2)$ and $\mu_1 = E_1/[2(1 + \nu_1)]$, and $u_{y,x} = 0$ is used. The equilibrium equation in the absence of body force in the x direction is written as:

$$\sigma_{x,x} + \tau_{xy,y} = 0. \quad (3)$$

Combining Eqs. 2 and 3, one obtains

$$\bar{E}_1 u_{x,xx} + \mu_1 u_{x,yy} = 0. \quad (4)$$

By using the method of separation of variables, the general solution is obtained as

$$u_x(x, y) = (A_1 e^{cx/h} + A_2 e^{-cx/h}) [B_1 \sin(dy/h) + B_2 \cos(dy/h)], \quad (5)$$

where A_1, A_2, B_1 and B_2 are constants to be decided by the boundary conditions. Moreover, $d = \sqrt{\bar{E}_1/\mu_1}c$, and x and y are normalized by the thickness of the film.

The symmetry of the geometry and the free upper surface provide

$$u_x(0, y) = 0; \quad u_{x,y}(x, h) = 0. \quad (6)$$

Applying the above boundary conditions in Eq. 5, one obtains

$$u_x(x, y) = B \sinh(cx/h) \cos[d(1 - y/h)]. \quad (7)$$

At both ends, stress $\sigma_x = -\bar{E}_1 \varepsilon_x^0$. Due to assumptions of Eq. 1, this boundary condition cannot rigorously be satisfied at every point. However, the total normal force should be zero, namely

$$\frac{1}{h} \int_{y=0}^h \sigma_x(\lambda, y) dy = -\bar{E}_1 \varepsilon_x^0. \quad (8)$$

The above weak form boundary condition provides a global control of the resultant force being zero at the cracked end, but the local stress distribution may not be accurate. Therefore, the singularity and the mixed mode of cracking are not presented through this solution. The substitutions of Eq. 7 into Eq. 2, and Eq. 2 into Eq. 8 provide

$$B = -\sqrt{\frac{\bar{E}_1}{\mu_1}} \frac{h \varepsilon_x^0}{\cosh(c\lambda/h) \sin d}. \quad (9)$$

Along the bottom of the film, the interfacial friction force gives a resistance to the displacement in the x direction (Xia and Hutchinson 2000; Timm et al. 2003), namely

$$\mu_1 u_{x,y}(x, 0) = k u_x, \quad (10)$$

where k is the spring coefficient, which depends on the performance of the interface and material properties of the substrate. In some special cases, k can be directly obtained as a material constant. Insertion of Eq. 7 into Eq. 10 provides

$$d \tan d = \frac{kh}{\mu_1}; \quad c = \sqrt{\frac{\mu_1}{\bar{E}_1}} d. \quad (11)$$

Thus, parameters d and c can be numerically solved. However, generally the film is fully bonded to the substrate, so the spring coefficient k is not given. Following Xia and Hutchinson (2000) method, comparison of the energy release rate with the exact solution provides

$$c = \frac{2}{\pi g(\alpha, \beta)}; \quad d = \sqrt{\frac{\bar{E}_1}{\mu_1}} c. \quad (12)$$

The detailed derivation of the above equation is given in Sect. 3. Here the function $g(\alpha, \beta)$ is illustrated in Fig. 2. It depends on Dundur's parameters, α and β , namely,

$$\alpha = \frac{\bar{E}_1 - \bar{E}_0}{\bar{E}_1 + \bar{E}_0}, \quad \beta = \frac{\mu_1(1 - 2\nu_0) - \mu_0(1 - 2\nu_1)}{2\mu_1(1 - \nu_0) + 2\mu_0(1 - \nu_1)}, \quad (13)$$

with $\bar{E}_0 = E_0/(1 - \nu_0^2)$ and $\mu_0 = E_0/[2(1 - \nu_0)]$. Figure 2 shows the function $g(\alpha, \beta)$ for $\beta = 0$ and $\beta = \alpha/4$ (Beuth 1992), respectively. For convenience of the simulation (performed later), $g(\alpha, \beta)$ is fitted by a function (see Fig. 2) as:

$$g(\alpha, \beta) \approx \frac{1.258 - 0.40\alpha - 0.26\alpha^3 - 0.30\alpha^4}{1 - \alpha}. \quad (14)$$

Figure 2 shows that the dependence of $g(\alpha, \beta)$ on β is weak except when α close to -1 (Xia and Hutchinson 2000). Thus, the fitted function in Eq. 14 will be used to approximate $g(\alpha, \beta)$ in the following simulations.

Combination of Eqs. 7, 9, and 11/12 provides a closed-form elastic solution for the reduced problem. Then, the total displacement and stress fields read

$$u_x(x, y) = \varepsilon_x^0 x + B \sinh(cx/h) \cos[d(1 - y/h)], \quad (15)$$

$$\sigma_x = \bar{E}_1 (\varepsilon_x^0 + Bc/h \cosh(cx/h) \cos[d(1 - y/h)]), \quad (16)$$

and

$$\tau_{xy} = \mu_1 B d/h \sinh(cx/h) \sin[d(1 - y/h)] \quad (17)$$

with B given in Eq. 9, d and c given in Eqs. 11 or 12.

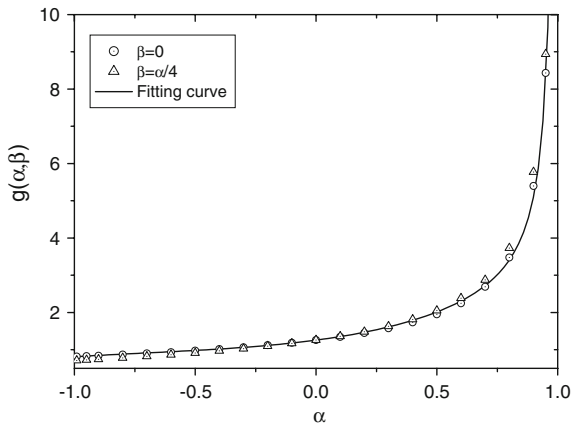


Fig. 2 The function $g(\alpha, \beta)$ versus α for $\beta = 0$ and $\beta = \alpha/4$ together with the fitting curve

If the substrate is much more compliant than the film, i.e. $E_0/E_1 \rightarrow 0$, the spring coefficient $k \rightarrow 0$. Then, from Eq. 11 we obtain $d \rightarrow 0$. Equation 12 will also give the same prediction of d . Substitution of Eq. 9 into Eq. 15 provides

$$\lim_{d \rightarrow 0} u_x(x, y) = 0. \tag{18}$$

Thus, the film has no deformation because the strain cannot be transferred to the film through the weak interface.

In addition, if the film is much more compliant than the substrate, i.e. $E_0/E_1 \rightarrow \infty$, the problem in Fig. 1b is reduced to the film attached on a rigid substrate, i.e. $k \rightarrow \infty$. Then, d in Eq. 11 can be explicitly solved as $d = \pi/2$.

Substituting Eqs. 9 and 19 into Eq. 15 yields the displacement field as

$$u_x(x, y) = \varepsilon_x^0 x - \sqrt{\frac{\bar{E}_1}{\mu_1}} h \varepsilon_x^0 \times \frac{\sinh(cx/h)}{\cosh(c\lambda/h)} \cos \frac{\pi(1-y/h)}{2}, \tag{20}$$

from which we can see that the x -directional strain along the bottom of the film is still constant as ε_x^0 . However, because d in Eq. 12 apparently depends on the Poisson’s ratio of the film, it seems that we cannot uniquely decide d as Eq. 19. This observation is not true. Because the dependence of $g(\alpha, \beta)$ on β is still considerable when $E_0/E_1 \rightarrow \infty$ or $\alpha \rightarrow -1$, which can be seen in Fig. 2, c in Eq. 12 will first change with the Poisson’s ratio of the film, and then Eq. 12 will

hopefully provide an identical d to Eq. 19 for varying Poisson’s ratio of the film. As an example, Beuth (1992) provided $g(-0.99, 0) = 0.8153$ and $g(-0.99, -0.25) = 0.7117$. For $\alpha = -0.99$ we obtain $E_0/E_1 = 199$; then, for $\beta = 0$ and -0.25 , we obtain $\nu = 0.5$ and 0.33 , respectively. From Eq. 12, d is obtained as 0.4971π and 0.4944π , respectively, from which we can predict d is approximately 0.5π for $\alpha \rightarrow -1$. Moreover, Eq. 12 shows that d only depends on material properties of the film/substrate system and is not related to the geometry of the film. In general, d is in the range of 0 to $\pi/2$, and the displacement field is also in between these two extreme cases.

3 Energy release rate and fracture toughness

Consider the section in Fig. 1b with two discontinuities at the both ends and with a large width compared to the thickness. When the external mechanical loading in the substrate increases, a steady-state channeling straight crack will initiate at the middle edge of the section and spread in the $-z$ direction as seen in Fig. 3. Far ahead the crack front, the elastic fields are not affected by the crack and are written in Eqs. 15–17. Thus the tensile stress at the symmetric plane is

$$\sigma_x(0, y) = \left(1 - \frac{d \cos[d(1-y/h)]}{\cosh(c\lambda/h) \sin d}\right) \sigma_x^0, \tag{21}$$

with $\sigma_x^0 = \bar{E}_1 \varepsilon_x^0$, and the shear stress is zero.

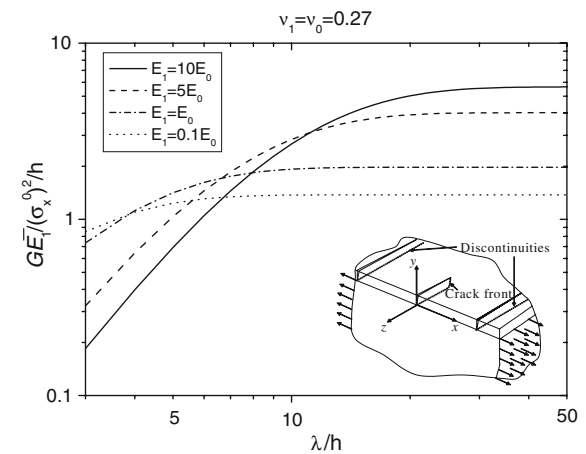


Fig. 3 Energy release rate of the crack front for a steady-state channeling crack in the section with large width and varying length

Far behind the crack front, the section is cracked into two pieces, and the elastic fields in each piece can also be solved by Eq. 15 with replacing λ by $\lambda/2$ in the new local coordinate system. Then we can solve the crack opening displacement as:

$$\delta(0, y) = 2\sqrt{\frac{\bar{E}_1}{\mu_1}} h \varepsilon_x^0 \frac{\tanh(\frac{c\lambda}{2h})}{\sin d} \cos[d(1 - y/h)], \quad (22)$$

To recover this crack opening displacement, the stress in Eq. 21 has to be applied along the cracking surface. Thus, the energy release rate of the crack front can be obtained as the work done to close the crack opening displacement (Beuth 1992), namely,

$$G = \frac{1}{2h} \int_0^h \sigma_x(0, y) \delta(0, y) dy. \quad (23)$$

Because the free boundary condition in Eq. 8 cannot rigorously be satisfied at every point along the crack surface, we use the averaged stress along the thickness to represent the local stress. Here we also use the averaged stress in Eq. 23, and then, the energy release rate can be explicitly written as

$$G = \frac{(\sigma_x^0)^2 h}{\bar{E}_1 c} \left[2 \tanh\left(\frac{c\lambda}{2h}\right) - \tanh(c\lambda/h) \right], \quad (24)$$

which provides the same form as Xia and Hutchinson (2000) results (see Eq. 30 of the paper) by setting $l = h/c$.

When the section is infinite long, i.e. $\lambda \rightarrow \infty$, Eq. 23 is reduced to

$$G = \frac{(\sigma_x^0)^2 h}{\bar{E}_1 c}. \quad (25)$$

Beuth (1992) also proposed the energy release rate averaged over the front of a semi-infinite isolated crack as

$$G = \frac{(\sigma_x^0)^2 h}{\bar{E}_1} \frac{\pi}{2} g(\alpha, \beta), \quad (26)$$

where $g(\alpha, \beta)$ can be further approximated by Eq. 14 as a function of α . These two cases should be equivalent (Xia and Hutchinson 2000), so that the following is obtained

$$c = \frac{2}{\pi g(\alpha, \beta)}. \quad (27)$$

This equation has been used to calibrate the constants c and d as Eq. 12.

Figure 3 shows the energy release rate at the crack front. Here $v_1 = v_0 = 0.27$ is used in the calculation. We can find that with the increase of λ , the edge

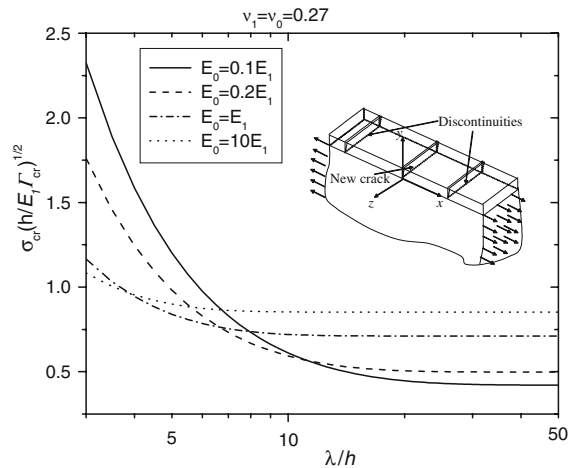


Fig. 4 Nominal tensile strength of the section with limited width and varying length

effect diminishes and thus the energy release rate is saturated at different lengths for different Young's modulus of the film. The higher the Young's modulus of the film, the larger the saturation length and the saturation energy release rate. Thus, cracks in a stiffer film interact across larger distances than vice versa. It is noted that the proposed model provides an identical prediction of the energy release rate to Xia and Hutchinson's (2000) model. Any errors in Eq. 24 follow from the assumption of Eq. 1 which is not accurate at the vicinity of the crack tip. This assumption will be further evaluated in Sect. 4.1.

For the section in Fig. 1b with a limited width, when the external mechanical loading reaches a critical value ε_x^{cr} , an unstable crack initiates at a flaw and quickly spreads across the width as seen in Fig. 4, and then the section is broken into two pieces. Thus, the fracture toughness of the film can be written as

$$\Gamma_{cr} = \frac{(\sigma_x^{cr})^2 h}{\bar{E}_1 c} \left[2 \tanh\left(\frac{c\lambda}{2h}\right) - \tanh(c\lambda/h) \right], \quad (28)$$

where the critical tensile stress $\sigma_x^{cr} = \bar{E}_1 \varepsilon_x^{cr}$ describes the nominal tensile strength of the film/substrate system. Thus, fracture energy can be measured through the measurement of the crack spacing λ and the critical value ε_x^{cr} . Here mechanical loading should be in the linear elastic range for both the film and the substrate. From Eq. 28, the nominal tensile strength can be written as:

$$\sigma_x^{cr} = \sqrt{\bar{E}_1 \Gamma_{cr}} \cdot \sqrt{\frac{c}{h}} \cdot \left(2 \tanh\left(\frac{c\lambda}{2h}\right) - \tanh(c\lambda/h) \right)^{-1/2}. \tag{29}$$

Because the fracture toughness is typically a material constant, once the fracture toughness of a material is obtained, we can use it to predict the general fracture behavior of the thin film under a tensile loading in the substrate. With further increasing the loading, the initiation of an additional crack can be determined by comparing the maximum averaged stress along the thickness of the film to the nominal strength given by Eq. 29. It is noted that the nominal strength is not only related to fracture toughness of the film and mechanical properties of the film and the substrate, but also decided by the geometry of the film.

Figure 4 illustrates the nominal tensile changing with the geometry of the film for a fully bonded film/substrate system. Here $v_1 = v_0 = 0.27$ is used. Figure 4 shows that the smaller the ratio of λ/h , the larger the nominal tensile strength; but when λ is large enough, the nominal strength is convergent to a constant. When λ/h is larger than 10, a compliant substrate provides a lower nominal strength because it cannot provide a strong support as a stiffer one. However, when λ/h is small, for example in the range of 3–4 in Fig. 4, the nominal strength for the compliant substrate is even higher than that for the stiffer one due to the large edge effect. When λ/h is fixed, from Eq. 29, the nominal strength changes with the thickness of the film as $\sigma_x^{cr} \propto \sqrt{1/h}$, which is consistent with the observation in the size effect experiments (Bažant 1999).

4 Results and discussion

A relatively extensive study of the proposed explicit elastic solution for a brittle film with periodic cracks is presented. The film is bonded to a substrate through either a frictional interface or a fully bonded interface. First, the proposed elastic solution is verified with FEM simulations. Using the solution, we investigate the following aspects: interfacial shear stress distribution, the effect of frictional spring coefficient, and edge effect on the energy release rate. As appropriate, our solution are compared to finite element results, results from other authors (e.g. Beuth 1992; Xia and Hutchinson 2000), and experimental results (Thouless et al. 1992).

4.1 Comparison with FEM simulations

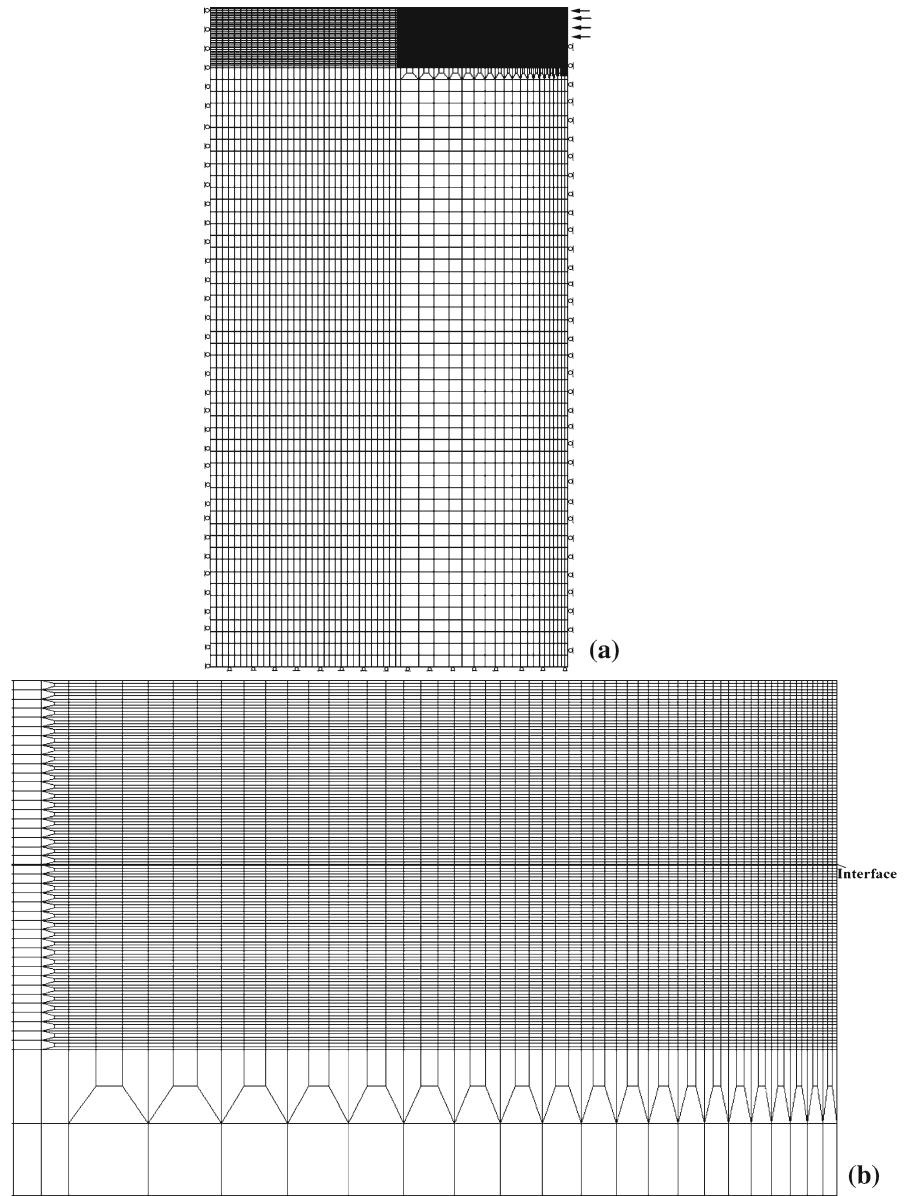
Because the problem in Fig. 1c is trivial, here only the reduced problem in Fig. 1d is considered. If this periodic section is extended to the total film, the geometry and the loading at a crack surface is same as the fully cracked problem of Beuth (1992) except that the former considers the periodically distributed discontinuities but the latter studies only one crack in films. From Eqs. 7 and 9, we can solve the work done by the external loading as

$$W = \frac{(\sigma_x^0)^2}{\bar{E}_1 c} h^2 \tanh(c\lambda/h). \tag{30}$$

To verify the integrity of the proposed analytical model, comparisons are made with the FEM simulation by ABAQUS. Two kinds of interfaces are considered. First, for a frictional interface, if the spring coefficient k is given, it is not necessary to consider the substrate. Due to the symmetry of the problem, only half of the section is modeled by 240×40 four-node quadrilateral elements with equal size under plane strain. This simulation is to show the reasonability of the plane assumption in Eq. 1. Secondly, a film fully bonded to the substrate is considered to simulate the real system. Because a singular point exists at the edge of the interface, the FEM mesh shown in Fig. 5 includes refined elements in the vicinity of that point. The x -directional displacement along the symmetric plane and the end of the substrate is constrained, which is consistent with Fig. 1d. Here the thickness of the substrate is 20 times as that of the film, and 11,260 four-node quadrilateral elements are used. To simulate the different length of the section, affine transformation of the mesh in the x -direction is used.

Figure 6 shows the external work calculated by Eq. 30 with comparisons to FEM simulations for two kinds of interfaces: a frictional interface and a fully bonded interface. With the increase of spring coefficient k or the Young’s modulus of the substrate E_0 , the external work reduces and is finally convergent to a constant. When the interface or substrate is stiff, for example, $k > 0.25$ or $E_0/E_1 > 1$, the cases of $\lambda = 12$ and $\lambda = 6$ provide the same result. Thus, the edge effect can be disregarded. However, when the interface or substrate is compliant, the case of $\lambda = 6$ gives a considerably lower result than that of $\lambda = 12$. Comparison of the theoretical predictions with the FEM results shows that the proposed model provides excellent agreement with the

Fig. 5 Finite element mesh used to model half of the geometry of the reduced problem: **a** total mesh, and **b** detail of refined mesh at the vicinity of the singular point



numerical simulations in Fig. 6a, which means that the assumption in Eq. 1 is reasonable for a frictional interface. However the proposed model provides a higher prediction for the fully bonded interface in the range of $E_0/E_1 < 1$ in Fig. 6b. The reason for this difference is that FEM simulation in Fig. 6b constrains the x -directional displacement at the crack tip whereas the proposed model permits this deformation. In Fig. 7b, we can clearly observe this difference: the displacement along the bottom of the film is zero at $x/\lambda = 1$ for the FEM results but it reaches the highest for the pro-

posed model. In the extreme situation, when $E_0/E_1 \rightarrow 0$, the boundary condition for FEM simulation is reduced to the beam under uniform compression with the bottom constrained at the both ends; whereas the proposed model is reduced to uniaxial compression of the beam. If the length of the section is permitted to be infinitely large, the half of the current problem is the same as Beuth (1992) problem. The external work for unit depth of the thickness in Eq. 30 is the same as Beuth's exact solution, which guarantees the accuracy of the proposed model for a film with large crack spacing.

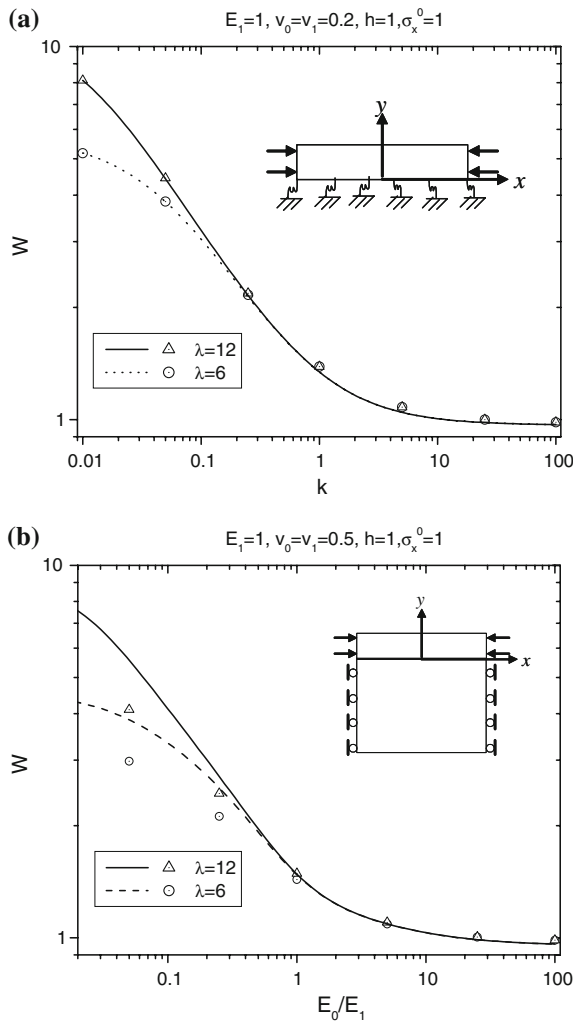


Fig. 6 Work done by the force along the ends of the film with two kinds of interfaces: **a** frictional interface with the varying spring coefficient, and **b** fully bonded interface with the varying Young's modulus of the substrate. Curves denote the theoretical predications; symbols the FEM results

The displacement distributions of u_x along the top and bottom of the films are shown in Fig. 7. It is seen that the stiffer the interface or substrate, the smaller the displacement field. The displacement field along the bottom of the film is always smaller than that along the top due to the constraint of the interface. In Fig. 7a, the displacement monotonically changes with x along both the bottom and the top of the film; whereas for the FEM simulations in Fig. 7b the displacement along the bottom of the film reaches the maximum in between and then decreases to zero at the end due to the strong

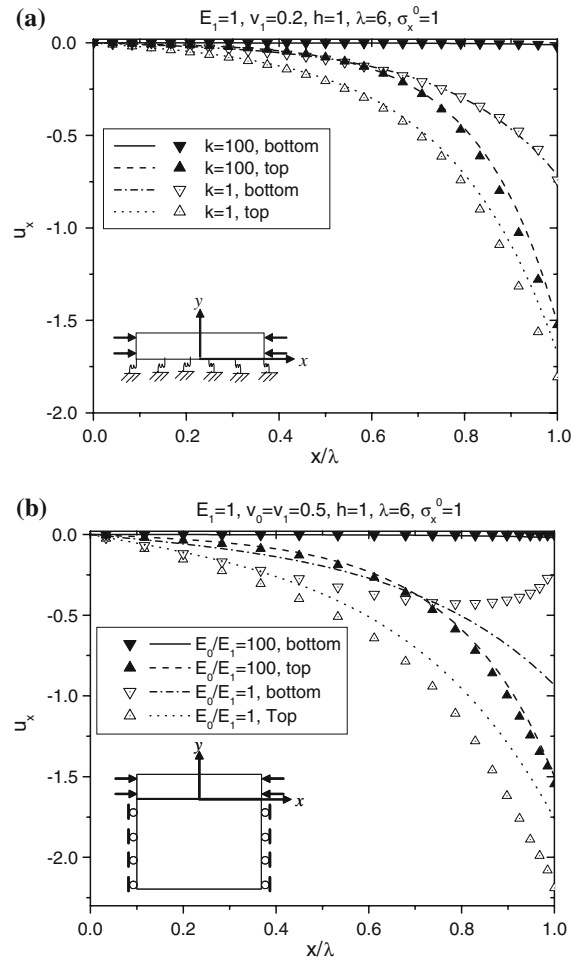


Fig. 7 Displacement field along the top and bottom of the film for two kinds of interfaces: **a** frictional interface with the spring coefficients $k = 1$ and 100 ; **b** fully bonded interface with the Young's moduli of the substrate $E_0 = E_1$ and $100E_1$. Curves denote the theoretical predications; symbols the FEM results

boundary condition. The proposed model provides a good agreement with the FEM results in Fig. 7a but it does not for the case of $E_0/E_1 = 1$ in Fig. 7b because boundary conditions for the FEM simulations and analytical derivation are different.

Figure 8 illustrates the interfacial shear stress distribution for two kinds of interfaces. In Fig. 8a we can find the theoretical solution well fits the FEM results even close to the end of the film for a frictional interface. However, for the fully bonded interface in Fig. 8b, due to the singular effect at the end of the film, the FEM provides a higher result in the neighborhood of singular point. In the other range, two methods still give

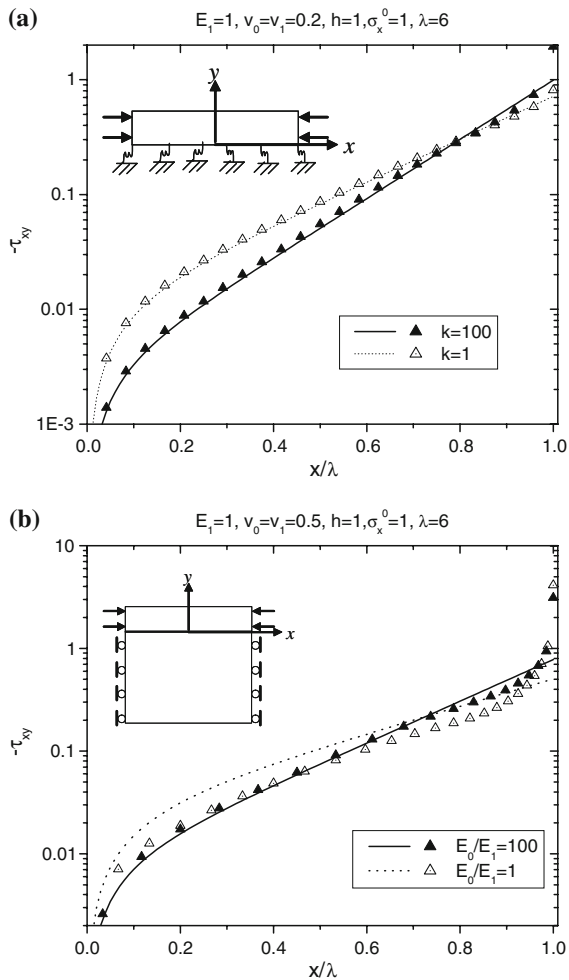


Fig. 8 Interfacial shear stress distribution for two kinds of interfaces: **a** frictional interface with spring coefficients $k = 1$ and 100; **b** fully bonded interface with the Young's moduli of the substrate $E_0 = E_1$ and $100E_1$. Curves denote the theoretical predications; symbols the FEM results

comparable predictions, especially for $E_0/E_1 = 100$. In the vicinity of the singular point, our assumption in Eq. 1 can not be rigorously satisfied, which also cause the approximate boundary condition in Eq. 8. Thus, the accuracy of this analytical solution cannot be guaranteed in this region.

Essentially, the proposed model is based on the assumption of the frictional interface. To accurately simulate the fully bonded interface, we followed Xia and Hutchinson (2000) method to make the energy release rate for both kinds of interfaces equivalent in Eqs. 25 and 26. Thus, this model provides a good prediction in terms of total strain energy or external work

for the fully bonded interface, but it does not accurately predict the local elastic field especially in the vicinity of the singular point. However, in an average sense, the proposed model produces a good estimate of the local solution for the fully bonded interface, besides that it gives a very accurate solution for the general frictional interface.

4.2 Interfacial shear stress and frictional spring coefficient

The interfacial shear stress distribution is very important for evaluation of the interfacial shear strength (Agrawal and Raj 1989; Chen et al. 2000; Wang and Qiao 2004; Leever and Godart 2008). Combining Eqs. 9 and 17, we obtain an explicit solution of the interfacial shear stress as

$$\tau_{xy} = -c\sigma_x^0 \frac{\sinh(cx/h)}{\cosh(c\lambda/h)}, \quad (31)$$

from which we can solve the interfacial shear stress for both the frictional interface and the fully bonded interface with c defined by Eqs. 11 and 12, respectively. Obviously, it is different from Agrawal and Raj (1989) assumption as they have used a sine-wave function to approximate the interfacial shear stress. Especially, for a thin film fully bonded to a rigid substrate, Eq. 12 combined with Eq. 19 produces $c = -\pi/2\sqrt{(1-\nu_1)}/2$. Substituting this quantity into Eq. 31, we can obtain the interfacial shear stress distribution for a film bonded to a rigid substrate. In Fig. 9, we see that at the singular point ($x/\lambda = 1$), the shear stress is almost same for each the ratio of h/λ because the thickness h is typically much smaller than the crack spacing and then $\tanh(c\lambda/h)$ is convergent to 1. The shear stress exponentially decrease from the singular point and is finally reduced to zero at the symmetric point. The smaller the ratio of h/λ , the larger the curvature of the curve. Thus, for a very thin film, the interfacial shear stress is only concentrated in the neighborhood of the singular point. When the shear strength along the interface is given, by comparing the maximum shear stress and the shear strength, we can evaluate the propensity of the interfacial debonding.

In Eq. 12, we find that c or d only depends on the material constants for a fully bonded film/substrate system. The interface can be simulated by a frictional interface with the equivalent spring coefficient denoted by Eq. 11, i.e.,

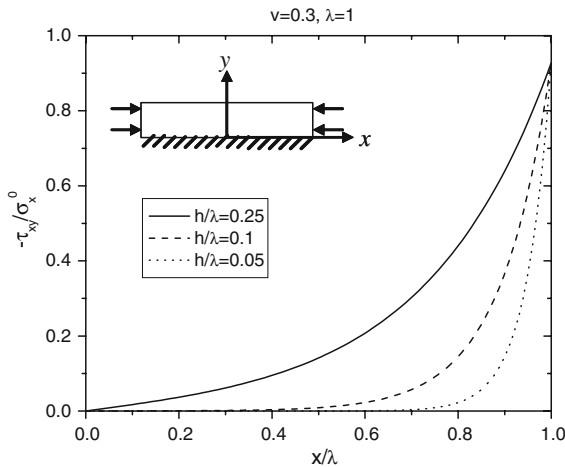


Fig. 9 Interfacial shear stress distribution for the thin film fully bonded to a rigid substrate with varying thickness $h/\lambda = 0.25, 0.1,$ and 0.05

$$k = \mu_1 d \tan d/h. \tag{32}$$

Obviously, the frictional spring coefficient of the interface will increase along with the decrease of the thickness of the film because μ_1 and d are material constants. Thus, the thinner the film, the stiffer the interface for the fully bonded film/substrate system. [Xia and Hutchinson \(2000\)](#) employed 1D solution to simulate the fully bonded interface and also obtained the equivalent spring coefficient (Eq. 12 of the Ref.) as

$$k = \mu_1 d^2/h. \tag{33}$$

Figure 10 illustrates the results of Eqs. 32 and 33. When $E_0/E_1 < 1$, two methods provide very close predictions. However, when $E_0/E_1 > 1$, the proposed method give a much higher prediction than [Xia and Hutchinson \(2000\)](#) method. We know that for a film bonded to a rigid substrate, i.e. $E_0/E_1 \rightarrow \infty$, the spring coefficient will be infinitely large. Obviously, [Xia and Hutchinson \(2000\)](#) method cannot predict this tendency, whereas the proposed method provides a very good explanation.

4.3 Edge effect on the energy release rate

In Sect. 3, we obtained the energy release rate for a channeling crack at the middle of the section. In reality, the crack may initiate at a flaw which is not exactly located at the middle point. Then the energy release rate cannot be solved by Eq. 24 due to the edge effect.

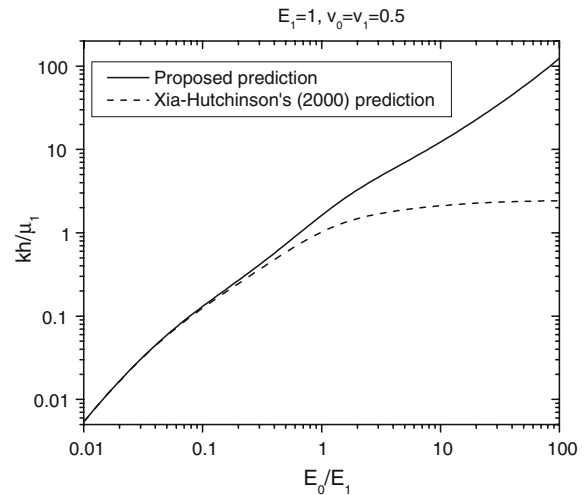


Fig. 10 Equivalent spring coefficients for a fully bonded interface with varying Young's modulus of the substrate

Here we consider that the crack is in the distance t to the symmetric plane as seen in Fig. 11. Following the same method in Sect. 3, we can write the tensile stress to close the crack as

$$\sigma_x(t, y) = \left(1 - \frac{d \cosh(ct/h) \cos[d(1-y/h)]}{\cosh(c\lambda/h) \sin d} \right) \sigma_x^0, \tag{34}$$

and the crack opening displacement as:

$$\delta(t, y) = \sqrt{\frac{\bar{E}_1}{\mu_1}} h \varepsilon_x^0 \frac{\tanh\left(c \frac{\lambda+t}{2h}\right) + \tanh\left(c \frac{\lambda-t}{2h}\right)}{\sin d} \times \cos[d(1-y/h)]. \tag{35}$$

Then, we can obtain the energy release rate as

$$G(t) = \frac{(\sigma_x^0)^2 h}{2\bar{E}_1 c} \left[\tanh\left(c \frac{\lambda+t}{2h}\right) + \tanh\left(c \frac{\lambda-t}{2h}\right) \right] \left(1 - \frac{\cosh(ct/h)}{\cosh(c\lambda/h)} \right). \tag{36}$$

Figure 11 shows the energy release rate for different locations of the crack with $c = 0.5$. The energy release rate of the crack front reaches the largest at the middle plane and is convergent to zero at the end of the section. The longer the section, the higher the energy release rate of the crack front at the middle plane. Moreover, the energy release rate changes more slowly in the middle range of the section for a longer section. For $\lambda/h = 24$, the energy release rate almost keeps constant as 1 in the range of $0 < t/\lambda < 0.5$; whereas for $\lambda/h = 6$, the energy release rate quickly falls down from 0.815 with the increase of t/λ . Therefore, when a

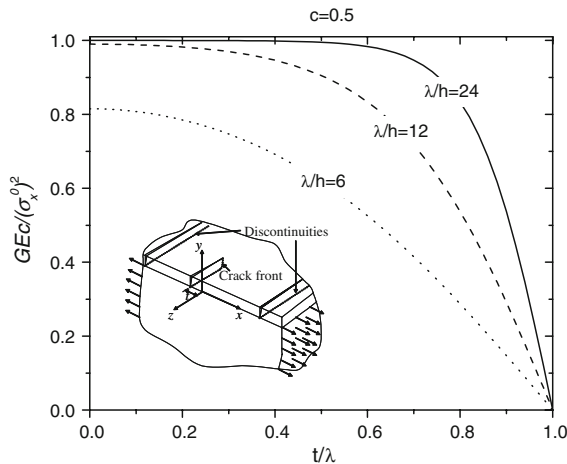


Fig. 11 Edge effect on the energy release rate of the crack front for a channeling crack with varying location

long film/substrate system is subjected to an increasing tensile loading on the substrate in the length direction, in the beginning, cracks will form in the middle range of the film, and many cracks may simultaneously initiate because the energy release rate can reach the maximum in a large range. After the film is cracked into many sections, the maximum energy release rate in each section will decrease so that it is smaller than the fracture toughness. When the tensile loading keeps increasing, the maximum energy release rate of the short section will reach the fracture toughness again and cause new cracks. When the length of the section is small enough, the new crack will initiate at the middle plane because the energy release rate at that location is considerably larger than that at other locations. Thus, finally the film will be cracked into the sections with the roughly equal length.

4.4 Crack spacing

A thin film/substrate system has widely been used to test the fracture quantities of the film by observation of the relation between the crack spacing and applied loading (Agrawal and Raj 1989; Thouless et al. 1992; Wang et al. 1998; Chen et al. 2000). The proposed model offers a convenient way to calculate the fracture energy or to predict the crack spacing from Eq. 28. To demonstrate the validity of the proposed method, we compare with the experimental data conducted by Thouless et al. (1992). They examined the PrBa₂

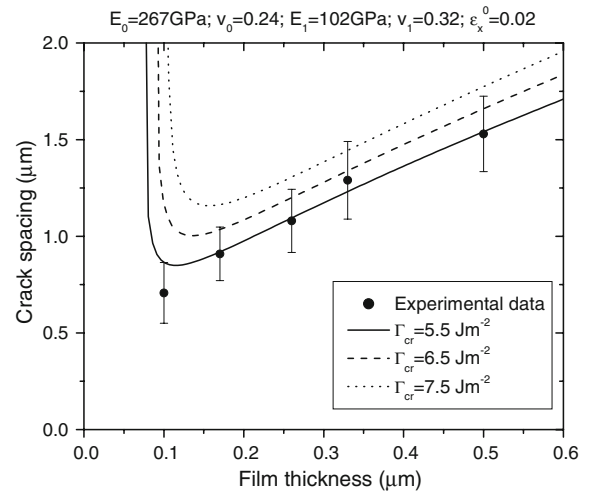


Fig. 12 Comparison of the experimental data (Thouless et al. 1992) for crack spacing as a function of film thickness with the proposed predictions for different fracture toughness of the film

Cu₃O_{7-x} films bonded to SrTiO₃ substrates and observed the relation between the crack spacing and the film thickness. Elastic constants for SrTiO₃ are given (Bell and Rupprecht 1963) as $E_0 = 267$ GPa and $\nu_0 = 0.24$ ($c_{11} = 317$ GPa and $c_{12} = 102.5$ GPa). The Young's modulus of PrBa₂Cu₃O_{7-x} and the tensile strain are given (Thouless et al. 1992) as $E_1 = 102$ GPa and $\varepsilon_x^0 = 0.02$ respectively. In numerical simulations, both the film and the substrate are assumed to be isotropic materials and the Poisson's ratio of the film is assumed as $\nu_1 = 0.32$. Using Eq. 12, we can solve $c = 0.631$.

Figure 12 shows a comparison of the experimental data (Thouless et al. 1992) for crack spacing as a function of film thickness with the proposed prediction for the fracture toughness of the film as $\Gamma_{cr} = 5.5$, 6.5 , and 7.5 Jm⁻², respectively. We see that the curve for $\Gamma_{cr} = 5.5$ Jm⁻² fits the experimental data very well, and thus we can assume it to be the measured fracture energy, which is slightly lower than the 6.5 Jm⁻² predicted by Thouless et al. (1992). Actually, the curve for $\Gamma_{cr} = 6.5$ Jm⁻² in Fig. 12 is still acceptable except for the small thickness as 0.1 μm. It is noted that Thouless et al. (1992) did not take into account of the mechanical properties of the substrate; but the proposed method consider them through the parameter c defined in Eq. 12. It is reasonable for a stiffer substrate to provide a stronger constraint for the film and then to produce a larger crack spacing in a general loading condition.

Figure 12 illustrates that with the increased film thickness, the crack spacing also becomes larger. However, a critical thickness exists for each curve of the fracture toughness, below which the crack spacing quickly increases to be infinite. Thouless et al. (1992) also observed that there were no cracks for a film with thickness $0.08\ \mu\text{m}$; whereas the proposed results for $\Gamma_{cr} = 5.5\ \text{Jm}^{-2}$ predicts the critical thickness $h = 0.081\ \mu\text{m}$. Thus, the crack spacing does not monotonically increase with the film thickness. It is noted that Thouless et al. (1992) also presented a prediction which is in excellent agreement with the experiments. However, this method only provides a monotonically increasing estimation, so it cannot directly predict critical thickness and an additional condition is needed to calculate it. In contrast, the proposed Eq. 28 not only gives a good prediction of the crack spacing, but also directly provides the critical thickness as

$$H_{cr} = \frac{c\bar{E}_1\Gamma_{cr}}{(\sigma_x^{cr})^2}. \quad (37)$$

from which we can find that the critical thickness is proportional to the fracture toughness of the film and the quantity of c . Thus if the substrate is more compliant, the critical thickness will be smaller.

5 Conclusions

A 2D explicit elastic solution is derived for one section between two discontinuities of the film with a frictional interface or a fully bonded interface. From this solution, we calculate the energy release rate of three-dimensional channeling cracks and obtain a method to measure the fracture toughness and the nominal tensile strength of the film through the relation between the crack spacing and the tensile strain in the substrate. Comparisons with the FEM simulations verify the integrity of the proposed solution. If the section is infinitely long, this solution in terms of the energy release rate is reduced into Beuth's exact solution for a fully cracked film bonded to a semi-infinite substrate.

The interfacial shear stress is explicitly given for two kinds of interfaces. For a very thin film, the shear stress is only concentrated in the neighborhood of the crack tip, and is quickly reduced to zero far from that point. A thinner film provides a higher equivalent spring coefficient. The 2D solution is compared with Xia and

Hutchinson (2000) results obtained from 1D solution, which shows that the proposed solution exhibits better physical meaning. The edge effect on the energy release rate is further discussed and the cracking procedure of a long film/substrate system is simulated. When a film/substrate system is subjected to a fixed tensile strain in the substrate, fracture toughness is calculated and compared with experimental data. Given the fracture toughness of the film and the tensile loading in the substrate, there exists a critical thickness, below which no crack will initiate.

Acknowledgements We acknowledge the financial support from the Federal Highway Administration National Pooled Fund Study 776 and from the National Science Foundation (NSF) under grant CMMI#0800805. The results and opinions presented herein are those of the authors and do not necessarily reflect those of the sponsoring agency. Authors would like to thank Professor John Hutchinson for his advice on the calculation of the energy release rate. We would also thank Dr. Seong Hyeok Song for his help with the FEM simulations.

References

- Agrawal DC, Raj R (1989) Measurement of the ultimate shear strength of a metal ceramic interface. *Acta Metall* 37: 1265–1270. doi:10.1016/0001-6160(89)90120-X
- Alaca BE, Saif MTA, Sehitoglu H (2002) On the interface debond at the edge of a thin film on a thick substrate. *Acta Mater* 50:1197–1209. doi:10.1016/S1359-6454(01)00421-9
- Bazant ZP (1999) Size effect on structural strength: a review. *Arch Appl Mech* 69:703–725. doi:10.1007/s004190050252
- Bell RO, Rupprecht G (1963) Elastic constants of Strontium Titanate. *Phys Rev* 129:90–94. doi:10.1103/PhysRev.129.90
- Beuth JL (1992) Cracking of thin bonded films in residual tension. *Int J Solids Struct* 29:1657–1675. doi:10.1016/0020-7683(92)90015-L
- Beuth JL, Klingbeil NW (1996) Cracking of thin films bonded to elastic-plastic substrates. *J Mech Phys Solids* 44:1411–1428. doi:10.1016/0022-5096(96)00042-7
- Bordet H, Ignat M, Dupeux M (1998) Analysis of the mechanical response of film on substrate systems presenting rough interfaces. *Thin Solid Films* 315:207–213. doi:10.1016/S0040-6090(97)00755-4
- Chen BF, Hwang J, Chen IF, Yu GP, Huang J-H (2000) A tensile-film-cracking model for evaluating interfacial shear strength of elastic film on ductile substrate. *Surf Coat Technol* 126:91–95. doi:10.1016/S0257-8972(99)00669-6
- Etzkorn EV, Clarke DR (2001) Cracking of GaN films. *J Appl Phys* 89:1025–1034. doi:10.1063/1.1330243
- Fleck NA, Qiu XM (2007) The damage tolerance of elastic-brittle, two-dimensional isotropic lattices. *J Mech Phys Solids* 55:562–588. doi:10.1016/j.jmps.2006.08.004
- Hu MS, Evans AG (1989) The cracking and decohesion of thin films on ductile substrates. *Acta Metall* 37:917–925. doi:10.1016/0001-6160(89)90018-7

- Hutchinson JW, Suo Z (1992) Mixed mode cracking in layered materials. *Adv Appl Mech* 29:63–191
- Leevers PS, Godart M-A (2008) Adiabatic decohesion in a thermoplastic craze thickening at constant or increasing rate. *J Mech Phys Solids* 56:2149–2170. doi:[10.1016/j.jmps.2008.02.001](https://doi.org/10.1016/j.jmps.2008.02.001)
- Liu XH, Suo Z, Ma Q (1999) Split singularities: stress field near the edge of a Silicon die on a polymer substrate. *Acta Mater* 47:67–76. doi:[10.1016/S1359-6454\(98\)00345-0](https://doi.org/10.1016/S1359-6454(98)00345-0)
- Malzbender J (2004) Stress profile and thermal expansion of layered materials determined from surface stresses. *Appl Phys Lett* 84:4661–4662. doi:[10.1063/1.1759773](https://doi.org/10.1063/1.1759773)
- Nakamura T, Kamath SM (1992) Three-dimensional effects in thin film fracture mechanics. *Mech Mater* 13:67–77. doi:[10.1016/0167-6636\(92\)90037-E](https://doi.org/10.1016/0167-6636(92)90037-E)
- Parmigiani JP, Thouless MD (2006) The roles of toughness and cohesive strength on crack deflection at interfaces. *J Mech Phys Solids* 54:266–287. doi:[10.1016/j.jmps.2005.09.002](https://doi.org/10.1016/j.jmps.2005.09.002)
- Saif MTA, Hui CY, Zehnder AT (1993) Interface shear stresses induced by non-uniform heating of a film on a substrate. *Thin Solid Films* 224:159–167. doi:[10.1016/0040-6090\(93\)90427-Q](https://doi.org/10.1016/0040-6090(93)90427-Q)
- Shenoy VB, Schwartzman AF, Freund LB (2001) Crack patterns in brittle thin films. *Int J Fract* 109:29–45. doi:[10.1023/A:1010973729754](https://doi.org/10.1023/A:1010973729754)
- Tadepalli R, Turner KT, Thompson CV (2008) Mixed-mode interface toughness of wafer-level Cu–Cu bonds using asymmetric chevron test. *Mech Phys Solids* 56:707–718. doi:[10.1016/j.jmps.2007.07.016](https://doi.org/10.1016/j.jmps.2007.07.016)
- Thouless MD, Olsson E, Gupta A (1992) Cracking of brittle films on elastic substrates. *Acta Metall Mater* 40:1287–1292. doi:[10.1016/0956-7151\(92\)90429-I](https://doi.org/10.1016/0956-7151(92)90429-I)
- Timm DH, Guzina BB, Voller VR (2003) Prediction of thermal crack spacing. *Int J Solids Struct* 40:125–142. doi:[10.1016/S0020-7683\(02\)00496-1](https://doi.org/10.1016/S0020-7683(02)00496-1)
- Vlassak JJ (2003) Channel cracking in thin films on substrates of finite thickness. *Int J Fract* 119/120:299–323. doi:[10.1023/A:1024962825938](https://doi.org/10.1023/A:1024962825938)
- Wang J, Qiao P (2004) Interface crack between two shear deformable elastic layers. *J Mech Phys Solids* 52:891–905. doi:[10.1016/S0022-5096\(03\)00121-2](https://doi.org/10.1016/S0022-5096(03)00121-2)
- Wang JS, Sugimura Y, Evans AG, Tredway WK (1998) The mechanical performance of DLC films on steel substrates. *Thin Solid Films* 325:163–174. doi:[10.1016/S0040-6090\(98\)00418-0](https://doi.org/10.1016/S0040-6090(98)00418-0)
- Xia ZC, Hutchinson JW (2000) Crack patterns in thin films. *J Mech Phys Solids* 48:1107–1131. doi:[10.1016/S0022-5096\(99\)00081-2](https://doi.org/10.1016/S0022-5096(99)00081-2)
- Yin HM, Buttlar WG, Paulino GH (2007) Periodic thermal cracking in an asphalt overlay bonded to a rigid pavement. *J Transp Eng* 133:39–46. doi:[10.1061/\(ASCE\)0733-947X\(2007\)133:1\(39\)](https://doi.org/10.1061/(ASCE)0733-947X(2007)133:1(39))
- Yu HH, He MY, Hutchinson JW (2001) Edge effects in thin film delamination. *Acta Mater* 49:93–107. doi:[10.1016/S1359-6454\(00\)00293-7](https://doi.org/10.1016/S1359-6454(00)00293-7)
- Zhao M-H, Fu R, Lu D, Zhang T-Y (2002) Critical thickness for cracking of $\text{Pb}(\text{Zr}_{0.53}\text{Ti}_{0.47})\text{O}_3$ thin films deposited on Pt/Ti/Si(100) substrates. *Acta Mater* 50:4241–4254. doi:[10.1016/S1359-6454\(02\)00254-9](https://doi.org/10.1016/S1359-6454(02)00254-9)